12TH CANADIAN CONFERENCE ON EARTHQUAKE ENGINEERING

12ÉME CONFÉRENCE CANADIENNE DU GÉNIE PARASISMIQUE

JUNE 17-20, 2019
CHÂTEAU FRONTENAC
QUÉBEC, QC.

17-20 JUIN 2019

CCEE 2019

Axial Load Effect on the Seismic Response of Reinforced Masonry Shear Walls with Boundary Elements

Nader Aly[1], Khaled Galal[2]

[1] Ph.D. Candidate, Department of Building, Civil and Environmental Engineering, Concordia University, Montréal, Québec, Canada.

[2] Professor, Department of Building, Civil and Environmental Engineering, Concordia University, Montréal, Québec, Canada.

ABSTRACT

It is well-known that high axial compressive load on structural walls limits the wall's curvature ductility and energy dissipation capacity. In Reinforced Concrete (RC) shear wall buildings, there are alternative structural systems (e.g. building frame system) that allow controlling the walls' share from vertical gravity forces. However, with the currently established construction techniques for Reinforced Masonry (RM) buildings, it is not practically recommended to utilize other than load-bearing walls as the structural system. Thus, RM shear walls in tall masonry buildings would be subjected to high axial compressive forces which will adversely affect its ultimate displacement capacity. Furthermore, the influence of axial compressive forces is more distinct on RM shear walls when compared to RC shear walls. Therefore, the primary objective of this study is to investigate the inelastic cyclic response of RM structural walls subjected to high axial compressive loads. In this respect, two half-scale fully grouted RM shear wall panels were constructed and tested under constant axial compressive load and in-plane fully reversed cyclic loading and top moment. The constructed walls have enlarged boundary elements made of C-shaped concrete masonry blocks which allowed meeting the seismic provisions of most design standards for the spacing of hoops to prevent the buckling of vertical reinforcement in the compression zone. In addition, these walls have a high aspect ratio and are flexural dominant in order to simulate the response of mid- and high-rise RM shear walls under severe seismic actions. The results of this study demonstrate that providing sufficient confinement in the RM boundary elements alleviated the impact of the high axial load on the walls' structural performance and resulted in a stable ductile response. Both walls which were subjected to axial pre-compression ratios higher than 10% were capable of attaining high levels of displacement ductility without significant loss in lateral resistance and failed in a flexure mode.

Keywords: RM shear walls, Boundary elements, Confinement, Axial load, Inelastic response.

INTRODUCTION

The increase in axial compression forces acting on shear walls increases its lateral strength but limits its displacement capacity. It was confirmed by past research studies and previous earthquake events that the adverse impact of axial load on displacement capacity and ductility outweighs the structural behaviour enhancements [1]. In Reinforced Concrete (RC) shear walls, even though extensive experimental studies have been performed in the past decades to quantify the influence of axial load, there is still a need for more experimental testing to understand the potential for buckling and low-cycle fatigue of vertical reinforcement bars under seismic loading [1]. RC shear wall buildings have the advantage of the possibility of utilizing a building frame structural system to reduce the axial compressive forces on the structural walls. In addition, several researchers, such as Su and Wong [2], highlighted that RC shear walls in medium and high seismicity regions are typically preferred to be designed with low axial load ratio to ensure a ductile response. However, in Reinforced Masonry (RM) buildings it is not practical to utilize other than wall load bearing structural systems. Thus, despite the possibility of reducing the axial load on RM shear walls by reducing the lengths of adjacent spans, RM shear walls in medium- and high-rise buildings would still be subjected to high levels of axial compressive forces due to gravity loads.

Su and Wong [2] tested three RC slender shear walls under constant axial load and reversed cyclic loading. The authors studied the impact of the axial load and confinement on the ductility capacity, energy dissipation, strength and stiffness deterioration and failure modes. The three tested specimens had identical geometrical configurations, constant longitudinal reinforcement ratio and a high aspect ratio of 4. The first two specimens (W1 and W2) had two different Axial Load Ratios (ALRs) of 0.25

and 0.5, respectively. The third wall (W3) was tested under the high ALR of 0.5 but with double the volumetric transverse reinforcement ratio provided in specimens W1 and W2. The test results indicated that, for the same confinement ratio, the experimental displacement ductility (μ_Δ) dropped by 33.7% (from 3.33 to 2.49) when the ALR was increased from 0.25 to 0.5. Furthermore, there was a clear reduction in the energy dissipation capacity attributed to the high ALR. It was also highlighted that high ALR resulted in a higher rate of strength degradation and axial stiffness deterioration. Finally, failure modes were found to be highly affected by the ALRs. The specimens with the high ALR (W2 and W3) had an out-of-plane brittle compressive failure characterized by cover spalling and inclined cracking in compressive zones. On the other hand, W1 (low ALR) failed in a flexural mode characterized by horizontal flexural cracks then concrete cover spalling followed by mild degradation in strength.

The experimental study by Banting and El-Dakhakhni [3] investigated the impact of axial load, among other parameters, on the response of RM shear walls with confined boundary elements built using stretcher blocks. Four walls were tested under quasi-static reversed cyclic lateral loading. The results of that study were used to establish the force- and displacement-based seismic performance parameters of RM shear walls with boundary elements. The results confirmed that boundary elements with two layers of vertical reinforcement and transverse reinforcement for confinement significantly improved the post-peak response. This is due to its ability in delaying the buckling of vertical rebars and providing confinement to the grout core. Therefore, the face-shell spalling and vertical cracking did not result in a significant drop in lateral capacity. Failure of tested walls occurred mostly due to the crushing of compression toes and fracture of vertical bars at high drift ratios ranging between 2.4% and 3.7% for the different walls. It was demonstrated that the increase in the axial load resulted in increasing the lateral resistance of the walls but limited its displacement ductility and drift capacities. The displacement ductility measured at ultimate displacement corresponding to 20% degradation in strength dropped by 34% when the axial pre-compression stress was increased from 0.89 MPa to 1.34 MPa (i.e. when the axial pre-compression ratio ($P/A_g f'_m$) increased from 5.4% to 9.8%). Additionally, the authors highlighted that the stiffness degradation was significantly influenced by the increase in the axial load.

It is clear that the axial compressive load on either RC or RM shear walls affects the cracking pattern, failure mode and the ductile response of the walls. It has an adverse influence on the curvature ductility, displacement ductility, stiffness degradation, strength deterioration and the energy dissipation capacity. The impact of the high axial compressive loads on the stiffness and strength degradation is more evident and perhaps more critical in RM shear walls. This is because it results in rapid face shell spalling as noted in the experimental testing by Shing et al. [4]. Up to the Authors knowledge, only the study by Banting and El-Dakhakhni [3] considered the impact of axial load on the structural response of RM shear walls with boundary elements. The primary objective of this study is to investigate the effects of the high axial compressive load on the inelastic response of RM structural walls with confined boundary elements built using C-shaped concrete masonry blocks. The focus is on evaluating the ability of utilizing confinement in the compression zone on mitigating the expected adverse effects of the high axial compressive loads. This is achieved by constructing and testing two RM shear walls with confined boundary elements subjected to high level of axial pre-compression ratios, top moment and reversed cycles of lateral displacements to simulate the expected response under seismic actions. The testing reported in this paper is part of an experimental program designed to evaluate the potential of utilizing RM shear walls with boundary elements in mid- and high-rise masonry buildings located in regions of moderate to high seismic hazard.
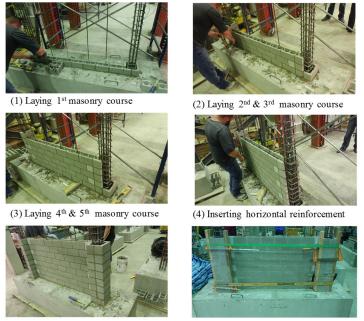
SPECIMENS DETAILS

The objective of this experimental program is to investigate the influence of the high axial compressive loads on the strength, stiffness, and displacement capacity of RM shear walls with confined boundary elements. For this purpose, two half-scale fully grouted RM shear wall panels were tested under constant axial load, and in-plane displacement-controlled fully reversed cyclic loading. The dimensions and reinforcement details of the tested walls are summarized in Table 1.

Table 1. Details of Tested Walls.

| Specimen | Wall Dimensions | | | Boundary Element | | | | | Web | | | | |
	Wall Length (mm)	Tested Panel Height (mm)	Height of First Story (mm)	Length (mm)	Width (mm)	Vertical bars	ρ_v (%)	Confinement	Thickness (mm)	Vertical bars	Horizontal bars	Axial Stress (MPa)
W1	1715	2380	1600	190	190	8#3	1.58	D4@60mm	90	4#3	D8@285 mm	2.25
W2	1725	2380	1600	290	190	8#3	1.03	D4@60mm	90	4#3	D8@285 mm	2.25

The tested walls represent a half-scale wall panel from a prototype 12-story building with a first-floor height of 3.2 m and a typical floor height of 3.0 m. The total half-scale height is 18.1 m, and the tested wall panel height was 2.38 m. The tested height simulates the plastic hinge region of the 12-story wall estimated as recommended by CSA S304-14 [5] clause 16 for the vertical extent of special detailing. The walls were tested under the same level of axial compressive stress of 2.25 MPa. The objective was to select an axial compressive load level that would result in neutral axis depths extending outside the small boundary elements (i.e. the 190mmx190mm boundary elements) and result in pre-compression ratios higher than 10%. The walls were designed and detailed in accordance to the requirements of CSA S304-14 [5], the design of masonry structures standard, to have a ductile flexural response. The walls presented in this study were constructed by a professional mason in the structures laboratory of Concordia University. The concrete masonry stretcher blocks used for the walls' web were half-scale replicas of the standard hollow 190mm concrete blocks commonly used in North America. All web stretcher blocks were depressed standard concrete masonry blocks to accommodate the horizontal rebars and allow the grout to flow smoothly and fill all the cells. The web blocks were laid in a running bond pattern with 5 mm Type-S mortar joints, whereas a stack pattern was used in constructing the boundary elements using the half-scale C-shaped blocks as shown in Figure 1. The walls were constructed and grouted at three stages to ensure the continuity of grout in all blocks' cells and to avoid having any discontinuity or voids in the walls. Two types of grout mix designs complying with the requirements of CSA A179-14 [6] were used. A high strength fine grout mix was used in the walls' boundary elements and an ordinary strength fine grout mix was applied in the walls' web.

(1) Laying 1st masonry course

(2) Laying 2nd & 3rd masonry course

(3) Laying 4th & 5th masonry course

(4) Inserting horizontal reinforcement

(5) Completing 1/3 of the wall height

(6) Strapping & grouting of 1st one-third

Figure 1. Construction sequence of the first 1/3 of specimen W1

Test setup and instrumentation

The tested walls are half-scale panels representing the plastic hinge region of 12-story RM shear walls. Thus, they were tested by applying lateral displacements at the top of the physical specimen in addition to top overturning moments to compensate for the height difference between the tested and actual walls. The lateral displacements were applied in a displacement-controlled mode at the RC loading beam level using a double-acting horizontal hydraulic actuator. The top moment and axial compression load were applied using two vertical hydraulic actuators in a force-controlled mode. The horizontal and the two vertical actuators were synchronized to apply the lateral displacement and the corresponding top moment. The test setup is shown in Figure 2, the three actuators were attached to a rigid steel frame. During the testing, the wall's out-of-plane displacements were restrained at the level of load application (i.e. at the RC loading beam) and at a level 1.6 m above the wall foundation. This level was selected to represent the first-floor slab and to limit the unsupported height-to-thickness ratio of the wall to 16, as suggested by CSA S304-14 clause 16.9.3 [5]. The out-of-plane support system was designed to allow translation and rotation since the tested specimens were subjected to lateral displacements and applied top moments.

The lateral displacements loading history used in testing the walls follows the fundamental requirements of quasi-static cyclic testing. As such, the size of the displacement increment was carefully proportioned, and the loading was applied slowly to allow ignoring the dynamic and strain-rate effects. The lateral displacement at the onset of the first yield in the outermost

vertical reinforcement was selected as the damage level. The experimental lateral displacement at yield (Δ_y) was estimated by recording the lateral displacement corresponding to the yielding strain measurement in any of the strain gauges installed at the vertical reinforcement rebars located at the wall-foundation interface. The applied loading protocol consisted of displacement-controlled fully reversed loading cycles, twice at each displacement level. The walls were first loaded with the constant axial compressive stress, simulating gravity loads, in a force-controlled mode, then the lateral cyclic displacements were applied at the middle of the top RC loading beam following the displacement-controlled loading history. The first portion of the loading history consisted of small increments (i.e., 25%, 50% and 75%) of the yield displacement (Δ_y), estimated based on the measured local strains in the vertical rebars at the wall-foundation interface, to capture the experimental displacement at the onset of the first yield. Subsequently, the loading history was defined as multipliers (i.e. 1, 2, 3 ...etc.) of the experimentally measured yield displacement (Δ_y). The measured lateral resistance at each displacement level was used to calculate the coupling forces (i.e., push/pull) in the vertical actuators to apply the corresponding top moment. The additional top moment is required to compensate for the height difference between the tested panel and the actual 12-story wall specimen. To sufficiently capture the post-peak response, the loading protocol displacement amplitudes were gradually increased until 20% strength degradation occurred or until any of the vertical rebars fractured and substantial crushing occurred in the grout core, whichever happened first. From the applied lateral displacements, the load-cell in the horizontal actuator measured the walls' lateral resistance.
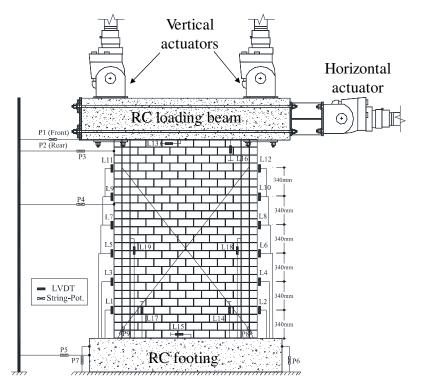

Figure 2. Test setup and external instrumentation

The tested walls were instrumented internally with 5-mm strain gauges, and externally with Linear Variable Displacement Transducers (LVDTs) and linear potentiometers. A total of twenty 5-mm strain gauges were used in each of the tested walls over the height of the two outer most reinforcement bars, at 40 mm into the bottom concrete footing, at the wall-foundation interface, at 758 mm, 1508 mm and 2273 mm from the wall-foundation interface. The strain gauges were used to measure the local strains in the reinforcement bars to estimate the extent of yielding over the wall height and the strain penetration into the bottom concrete footing. Furthermore, the strain gauges attached to the reinforcing bars at the wall-foundation interface were used to capture the yield displacement (Δ_y) which was then used to calculate the target displacements in the loading protocol. Nineteen LVDTs (L1-L19) were attached to the tested walls as shown in Figure 2 to measure the vertical displacements, any sliding shear displacements, and any uplift at the wall-foundation interface. Besides, eight linear potentiometers (P1-P8) were attached to measure the lateral displacements, any slip displacements and diagonal (shear) deformations.

PERFORMANCE QUANTIFICATION

Damage progression

Wall W1 had 8 No. 3 bars in a square 190 mm boundary element confined using D4 hoops spaced at 60 mm, whereas wall W2 had 8 No. 3 bars in a rectangular 190 mm x 290 mm boundary element. Both walls were subjected to the same high axial pre-

compression ratios. Figure 3 presents the load-displacement hysteresis loops of the two tested specimens. The forces shown in Figure 3 were corrected to account for the horizontal force component applied by the vertical actuators due to its inclination at higher lateral displacements. Moreover, the lateral displacements are reported at the top of the tested specimen, which represented the plastic hinge zone where all plastic deformations are concentrated. It can be seen that both specimens had almost a linear elastic response until the onset of the first yield in the outermost vertical reinforcement. The linear response was accompanied with thin hysteresis loops reflecting a low-level of energy dissipation. At higher lateral displacements, the response of the walls started to become nonlinear after the yielding of vertical reinforcement and the flexural horizontal cracks. Fatter hysteresis loops were seen indicating the increase in the energy dissipated by the walls through yielding of reinforcement and damage to masonry. As depicted in Figure 3, the two specimens had a very stable hysteretic response that is nearly symmetric in the push and pull directions. The second cycle at each displacement level did not result in any evident degradation in neither the lateral resistance nor the stiffness. The two loops are almost overlapping reflecting minor in-cycle degradation.
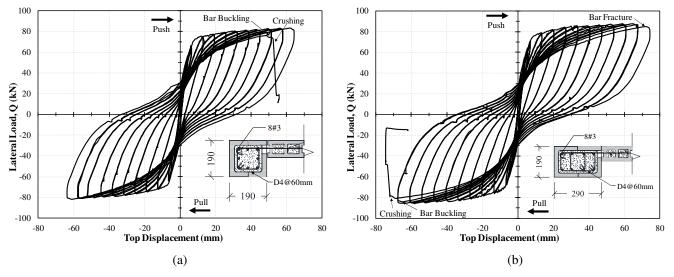

(a)   (b)

Figure 3. Lateral load-top displacement hysteresis loops: (a) wall W1, (b) wall W2

In wall W1, the average (for the push and pull directions) measured displacement at the onset of first yield (Δ_y) was 6.38 mm and the corresponding average lateral force (Q_y) was 65.13 kN. At the onset of the first yield in vertical reinforcement, there were few hairline horizontal flexural cracks along the bed joints in both sides of the wall. At the lateral displacement level of ($2\Delta_y$), which corresponds to 12.7 mm top displacement, the majority of horizontal cracking along the bed joints were in the first story of the wall (i.e. up to the first level of out-of-plane support). The number of bed joint horizontal cracks continued to increase with the progression of the loading history, and the cracks were mainly concentrated in first-story of the wall. The first vertical crack was initiated in the left boundary element at the lateral displacement level of ($5\Delta_y$) (i.e. 31.9 mm top displacement). The vertical crack extended up over two masonry courses in the corner of the left boundary element. At the end of the second push to the displacement level of ($6\Delta_y$), a top displacement of 38.3 mm, the vertical crack in the left boundary element propagated to the fourth course with a bigger width. After the second pull at the same displacement level, the masonry face-shell spalling was initiated in the first three courses of the left boundary element that cracked during the push cycle. No new horizontal cracks were observed after this displacement level in the first-story, only a few diagonal shear cracks developed, and existing horizontal cracks were propagating. The vertical crack in the left boundary element propagated up the height of the wall until the sixth course at the top displacement of 44.7 mm (i.e. at $7\Delta_y$). Moreover, vertical cracking was initiated in the right boundary element over the first four courses combined with toe crushing at the same drift level of ($7\Delta_y$). Furthermore, few horizontal cracks in the bed joints were observed in the top floor above the out-of-plane support level. At the end of the second loading cycle at ($8\Delta_y$), face-shell spalling was observed in both left and right boundary elements with toe crushing in both sides in the first course. It is interesting to highlight that the spalling of boundary elements' face-shell did not result in any lateral strength degradation. After two loading cycles at ($9\Delta_y$), which corresponds to a top of tested wall displacement equal to 57.4 mm, face-shell spalling propagated up to the 6th masonry course in the left boundary element. Furthermore, crushing in the left boundary element grout core was observed along with vertical cracks. Two vertical reinforcement bars were exposed in the left boundary element between the hoops in the 2nd and 3rd courses. The exposed vertical reinforcement started to buckle between the hoops in the 3rd masonry course during the first push in the ($10\Delta_y$) loading cycle (i.e. at a top of wall displacement of 63.8 mm), as shown in Figure 4(a). In the second push to the lateral displacement corresponding to ($10\Delta_y$), substantial crushing was seen in the grout core of the left boundary element at the level of buckled vertical reinforcement. This was followed by buckling of the majority of the vertical rebars in that level (i.e. 3rd course in the left boundary element). The grout core crushing extended to the wall web causing buckling of the closest web vertical rebar to the boundary element. A sudden significant loss of lateral

resistance was observed, and the test was terminated. Thus, wall W1 failed in a flexural-mode, characterized by significant horizontal cracks, due to buckling of the vertical reinforcement and crushing of the grout core in the left boundary element at a top of wall displacement equal to 63.8 mm. The final damage state of W1 at a displacement ductility factor (μ) of 10 is shown in Figure 4(b), and the failure mode of the left boundary element is presented in Figure 4(a).
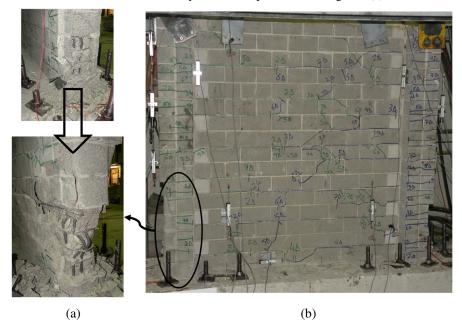

| (a) | (b) |

Figure 4. Wall W1: (a) failure mode at displacement-ductility (μ) of 10, (b) final damage state

Specimen W2 had an average lateral displacement at the onset of yield equal to 6.75 mm and the average corresponding lateral force at first yield (Q_y) was 69.23 kN. At the onset of first yield displacement, only minor hairline horizontal cracks occurred in the bed joints in both sides of the wall. After the two loading cycles at the displacement level of ($2\Delta_y$), 13.5 mm displacement at top of tested wall, there was a significant number of horizontal cracks in the bed joints extending along the wall's length and few horizontal hairline cracks in the boundary element blocks. All the cracks were concentrated in the first-story under the first level of out-of-plane support. At the second push in the loading cycle of ($6\Delta_y$) which corresponds to 40.5 mm top displacement, toe-crushing was visible in the left side, and vertical cracks were observed in the first five courses in the left boundary element. After the completion of the second pull cycle, vertical cracks and toe-crushing were also seen in the right boundary element. At the end of the two-loading cycle at $6\Delta_y$, the spalling of face-shells was seen in the first five courses of the left boundary element and the first four courses of the right boundary element. After the two loading cycles at ($7\Delta_y$), vertical cracks propagated over the height of the right boundary element resulting in face-shell spalling up to the 8th masonry course in the right boundary element and up to the 6th masonry course in the left boundary element. The face-shell spalling did not cause any degradation in the lateral resistance of the wall. It is worth mentioning that after the lateral displacement corresponding to ($5\Delta_y$) no new cracks were visible, only opening and closure of existing horizontal and diagonal cracks was seen. During the two cycles to the top displacement of 54 mm (i.e. $8\Delta_y$), toe-crushing was seen in both left and right boundary elements. Furthermore, vertical cracks and crushing were observed in the grout core of 2nd course in left boundary element and 2nd and 3rd courses of right boundary elements. After the first loading cycle to the displacement level of ($9\Delta_y$), crushing of grout core and cover spalling was observed in left and right boundary elements' 2nd and 3rd courses. At the end of the second cycle to ($9\Delta_y$), corresponding to 60.8 mm top displacement, the outermost vertical rebar buckled between the hoops in the 2nd-3rd courses of the right boundary element causing spalling of the grout core cover. During the first push to $10\Delta_y$, face-shell spalling of the 6th to 13th masonry courses was observed in the left boundary element. In the first pull, the exposed vertical bar in the right boundary element buckled again. Further buckling in that bar occurred in the 1st and 2nd pull cycles to the lateral top displacement of 67.5 mm (i.e. $10\Delta_y$). In addition, another vertical bar buckled in the right boundary element and a vertical bar was exposed in the left boundary element due to spalling of grout core cover in the 3rd masonry course. In the first push to ($11\Delta_y$), top displacement of 74.3 mm, the buckled vertical rebar in the right boundary element fractured, as shown in Figure 5(b), due to low-cycle fatigue effect. The repeated buckling softened the material of the rebar causing a reduction in its fatigue life and resulting in fracture of the rebar [7]. At the peak of the first pull in the loading cycle to ($11\Delta_y$), as illustrated in Figure 5(b), extensive crushing occurred in the right boundary element core, and vertical cracks started to propagate over the boundary element height. Moreover, the crushing propagated to the wall web causing a vertical bar to buckle in the web. The wall failed at this displacement level which corresponded to a displacement ductility factor (μ) of 11 due to a substantial loss in lateral resistance triggered by the crushing of the compression zone, as illustrated in Figure 5. Therefore, specimen W2 exhibited a ductile flexural response seen in the

significant horizontal cracking, yielding of vertical reinforcement, spalling of masonry face-shell, buckling and subsequent fracture of vertical rebar along with the crushing of the grout core.
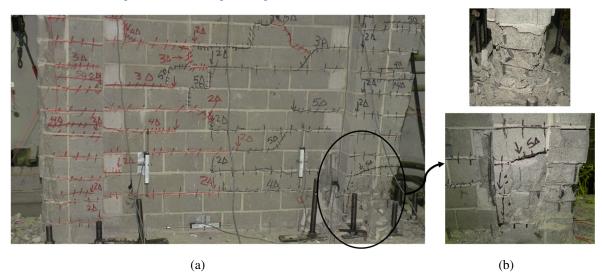

<table>
<tr><td>(a)</td><td>(b)</td></tr>
</table>

Figure 5. Wall W2: (a) final damage state, (b) failure mode at displacement-ductility (μ) of 11

Lateral load and displacement capacities

The lateral load-displacement envelop curves of walls W1 and W2 are shown in Figure 6. Both walls had a stable cyclic response; the walls were capable of preserving their lateral strength until either extensive crushing in the grout core combined with buckling of several vertical rebars (W1) or until fracture of a vertical rebar and a subsequent substantial crushing in the grout core (W2). W1 had an ultimate resistance (Q_u) of 83 kN in the push direction and -82 kN in the pull direction measured at a lateral top displacement of 63.8 mm. This reflects a symmetric response for the wall in both loading directions and implies a uniform fully grouted section with no discontinuous or cavities. Similarly, specimen W2 had a symmetric response with peak resistances (Q_u) of 88 kN and -86 kN in the push and pull directions recorded at a corresponding top of wall displacement equal to 60.8 mm.
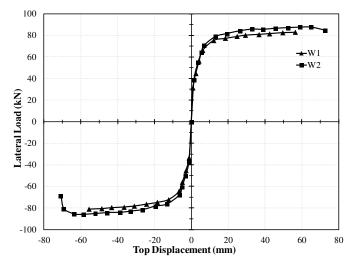

Figure 6. Lateral load-top displacement skeleton curves

As illustrated in Figure 6, specimens W1 and W2 had a hardening response until top of wall drifts ratios higher than 2.0%. W2, which had a rectangular 190 mm x 290 mm boundary element, had a slightly higher average lateral resistance by 5% compared to W1. The predicted and average measured yield (Q_y) and ultimate lateral (Q_u) forces of walls W1 and W2 are summarized in Table 2. The strength predictions were calculated using CSA S304-14 [5] flexural strength equations and assuming no material strength reduction factors. Besides, the strength calculations accounted for the effect of strain-hardening in reinforcing steel on the capacity. The contribution of the compression reinforcement to the lateral resistance was also accounted for, but only for the rebars that were sufficiently tied using the confinement hoops. Both yield and ultimate resistances were underestimated,

especially for the wall with the larger confined grout core (i.e. W2). The yield capacity was underestimated by 9% and 20% for walls W1 and W2, respectively. Ultimate resistance predictions were slightly underestimated by 6% for W1 and 8% for W2. Thus, overall the prediction of capacities based on the application of beam analysis theory and using the equations of CSA S304-14 [5] including the tied compression reinforcing bars was acceptable. The experimental displacement ductility (μ), calculated as the ratio between the measured lateral displacement at the onset of first yield and the ultimate displacement was 9.7 for W1 and 10.7 for W2. Therefore, the increase in the confined grout core size only resulted in a marginal increase of 10% in the displacement ductility of the wall and 5% enhancement in the lateral resistance.

Table 1. Predicted and measured walls' lateral capacities.

Specimen	Predicted		Measured	
	Q_y (kN)	Q_u (kN)	Q_y (kN)	Q_u (kN)
W1	60	78	65	83
W2	58	80	69	87

CONCLUSIONS

The experimental results reported in this paper demonstrate the capability of RM shear walls with confined boundary elements, made up using C-shaped concrete masonry blocks, subjected to axial pre-compression ratios higher than 10% of achieving a stable ductile response. Both tested specimens were capable of attaining high levels of displacement ductility without significant loss in lateral resistance. Although the two walls were subjected to a high axial compressive load, the two walls failed in a flexural mode due to extensive crushing in the grout core and low-cycle fatigue failure in vertical reinforcing bars. This was due to the ability of the provided confinement in the compression zone of the walls (i.e. the boundary elements) in limiting the adverse influence of the high axial pre-compression and the resulting face-shell spalling on the lateral resistance and displacement ductility of the walls. The presence of sufficient confinement in the boundary element eliminated the impact of face-shell spalling on both walls' vertical and lateral load carrying capacity. Besides, it delayed the buckling of vertical reinforcement and restricted its impact on lateral resistance until substantial crushing occurred in the grout core. It was possible to conservatively predict the lateral load at the onset of first yield and the ultimate resistance of the two specimens using CSA S304-14 [5] flexural strength equations. Based on the results, it is also concluded that increasing the size of the confined grout core, i.e. increasing the volumetric ratio of confinement reinforcement, resulted in 5% enhancement in the lateral resistance and 10% improvement in the deformation capacity measured at ultimate displacement. Furthermore, increasing the confined grout core size was effective in restricting the buckling of vertical rebars from resulting in a significant loss of lateral capacity.

ACKNOWLEDGMENTS

REFERENCES

[1]   Yuen, Y., and Kuang, J. (2014). "Axial compression effect on ductility design of reinforced concrete structural walls." In *Second European Conference On Earthquake Engineering and Seismology*, Istanbul, Turkey.

[2]   Su, R. K. L., and Wong, S. M. (2007). "Seismic behaviour of slender reinforced concrete shear walls under high axial load ratio." *Engineering Structures*, 29(8), 1957–1965.

[3]   Banting, B. and El-Dakhakhni, W. (2012). "Force- and displacement-based seismic performance parameters for reinforced masonry structural walls with boundary elements." *Journal of Structural Engineering*, 138 (12), 1477–1497.

[4]   Shing, P. B., Klamerus, E., Spaeh, H., and Noland, J. L. (1988). "Seismic performance of reinforced masonry shear walls." In *9th World Conference on Earthquake Engineering*. Tokyo-Kyoto, Japan, 6, 103-108.

[5]   Canadian Standards Association-CSA (2014). CSA-S304-14: *Design of masonry structures.* Prepared by the CSA, Mississauga, Ontario, Canada.

[6]   Canadian Standards Association-CSA (2014). CSA-A179-14: *Mortar and grout for unit masonry.* Prepared by the CSA, Toronto, Ontario, Canada.

[7]   Kunnath, S. K., and Brown, J. (2004). "Low-cycle fatigue failure of reinforcing steel bars." *ACI Materials Journal.*, 101(6), 457–466.